# The anodic behavior of Alloy 690 in simulated PWR primary water at 290°C

Tichun Dan[a, b], Kazuhko Sakaguchi[a], Zhanpeng Lu[a], Tetsuo Shoji[a],
Jianqiu Wang[b], Eenhou Han[b], Wei Ke[b]

a) Tohoku University Fracture and Reliability Research Institute, Japan
b) Institute of Metal Research (IMR), Chinese Academy of Sciences (CAS), China

This study investigates the anodic behavior of Alloy 690 thermal treated (TT) in Pressurized Water Reactors (PWRs) primary water at 290°C, 9 MPa by means of polarization measurement, electrochemical impedance spectroscopy (EIS) and X-ray photoelectron spectroscopy (XPS) analysis. Experimental results of hydrogen charged and uncharged Alloy 690TT show that hydrogen increases anodic steady current density and decreases capacitance loop, which implies that charged hydrogen changes the electrochemical processes in the growth of oxide film. Elemental distribution along depth profile by XPS analysis indicates that oxide film increases after hydrogen charging at $0.277V_{SHE}$ ($0.3V_{Ag/AgCl}$) and this changing of outer layer of the oxide film is unrelated to oxidation of chromium and hydrogen maybe accelerate oxidation of nickel and iron. Charged hydrogen probably accelerates oxidation of chromium in the inner oxide layer.

**Keywords**: Alloy 690, hydrogen, anodic polarization, EIS, M-S plot, XPS

## 1. Introduction

Inconel Alloy 690(Ni60-Cr30-Fe10) has been selected for use in Pressurized Water Reactors (PWR) nuclear power plant materials such as steam generator tubes due to their good resistance to stress corrosion cracking and pitting resistance in pure water at high temperatures and pressures. Hydrogen is known to play a major role in some stress corrosion cracking (SCC) phenomena especially intergranular stress corrosion cracking (IGSCC) of nickel-base alloy [1-7] but its precise role in oxide or passive film degradation mechanism remains to be un-fully understood. This is particularly the case in the nuclear industry for the SCC of nickel base alloys occurring in pressurized-water reactors (PWRs). Some researchers reported that the growth of oxide film, composed of outer Fe-rich layer overlying an inner Cr-rich layer, followed logarithmic kinetics and 1.0 ppm of dissolved hydrogen (DH) corresponded to NiO/spinel oxide boundary in phase diagram, and the oxide film was relatively less protective in that case [8, 9]. The hydrogen so dissolved could then enter the metal and consequently affect its electrochemical behavior. Few, if any, investigations have stressed the correlation between the hydrogen and electrochemical behavior of nickel-base alloy, especially in hydrogenated PWR water [4].

In the present investigation, we report on the effects of hydrogen on the anodic polarization and passivity behavior of alloy in a simulated PWR primary water at 290°C by polarization curve, electrical impedance spectroscopy (EIS), and Mott-Schottky plot measurements. Surface morphologies are observed by Scanning Electron Microsopy (SEM) and the elemental distribution of depth profile for oxide film is analyzed by X-ray photoelectron spectroscopy (XPS).

## 2. Experimental

### 2.1 Materials and solutions

The composition of Alloy 690 used (wt%) is: C 0.025, Si 0.22, Mn 0.32, P 0.003, S 0.005, Ni 59.6, Cr 30.5, Mo 0.02, Fe 9.3, N 0.002. Heat treatment was mill annealed at 1075°C and thermal treated at 700°C for 15 hours. The Alloy 690 TT bulk was made by one-dimension (1D) cold worked (CW) 25%. For base metal Alloy 690TT, its yield strength (0.2% proof) and tensile stress at RT were 243 MPa, 573 MPa and 641 MPa, 690 MPa for 1D CW Alloy 690 TT. 1D CW Alloy690 TT is used in the test. Samples were cut into 10×10 ×2 mm coupons and dot-welded to a stainless steel wire surrounding with colorless shrinkable Teflon. All of the specimens were ground mechanically with emery papers up to 1500 grit, and then rinsed using de-ionized water and ethanol successively.

Solutions were made by high-purity water and analytical-grade reagents. The test solutions are made by

1200ppm B in $H_3BO_3$ with 2ppm Li in LiOH. The temperature and dissolved hydrogen (DH) are invariably controlled at 320°C and 30cc/kg (2.6ppm), respectively.

### 2.2 Electrochemical cell setup

All the hydrogen charging and electrochemical measurements were performed in an autoclave equipped with a re-circulating loop. A three-electrode cell was used for electrochemical measurement. In the system, a calibrated Ag/AgCl electrode was used as a reference electrode and platinum electrode was used as a counter electrode. A two-electrode cell was used for hydrogen charging. For hydrogen charging, twisting platinum (Pt) wire was used as a counter electrode and hydrogen charging current density was -0.5mA/cm$^2$. Potentials cited in this paper were all referred to Ag/AgCl electrode and converted to Standard Hydrogen Electrode (SHE) according to Mcdonald's equation [10]. Potentiostatic measurements were recorded with a Solartron SI 1287 electrochemical interface. Scan rate of anodic polarization measurements was 50mV/min, scanning from open circuit potential (OCP). Electrical impedance spectroscopy (EIS) measurements were carried out with SI 1260 Impedance/Gain-Phase Analyzer. The amplitude of the AC signal was 10 mV, and the test frequencies ranged from 10,000 Hz to 0.005 Hz. Current density *vs.* time at 0.277$V_{SHE}$ (0.3$V_{Ag/AgCl}$) and EIS measurements at open circuit potential(OCP) were made after H-charging for 50h. Mott–Schottky plots of the immersed samples were measured using the SI 1287 electrochemical interface equipped with the SI 1260 frequency response analyzer (FRA, Solatron, Inc.) with a constant frequency of 1 kHz。The measurement potential was scanned from -0.923$V_{SHE}$ (-0.9 $V_{Ag/AgCl}$) to 1.177$V_{SHE}$ (1.2 $V_{Ag/AgCl}$). After the hydrogen charging, the current density *vs.* time measurements, current responses of the specimens at 0.277$V_{SHE}$ (0.3$V_{Ag/AgCl}$) were recorded immediately.

### 2.3 Surface analysis

S-4700 Scanning Electron Spectroscopy (SEM) was used to observe surface morphology after high-temperature electrochemical measurements. Immersed samples were dried by ethanol before SEM observation. X-ray photoelectron spectroscopy (XPS) analyses were carried out using Quantum 2000 Scanning ESCA Microprobe to examine the passive film formed on the Alloy 690TT. The X-ray source was the Kα peak of aluminum. An incidence angle to the specimen was 45° and the the analyzing area was 100μm × 100μm.

## 3. Results and discussion

### 3.1 Effects of hydrogen on the anodic polarization

Anodic polarization curves of uncharged and charged samples were shown in Fig. 1. After hydrogen charging, corrosion potential negatively moved to -1.013$V_{SHE}$ (-0.99$V_{Ag/AgCl}$) from -0.453$V_{SHE}$ (-0.43$V_{Ag/AgCl}$) and quasi-steady current density increased to 40.92μA/cm$^2$ from 15.63μA/cm$^2$. It should be considered that the potential of reference electrode would shift with a constant value during measurements. The quasi-steady current density is approximately considered passive current density corresponding to the typical polarization curve. For comparison, Pt electrode was charged to make anodic polarization. Effects of hydrogen on the anodic behavior of Pt electrode were negligible. After anodic polarization, observed surface morphology indicated that particles were present on the surface and some slight intergraular attack (IGA) and seemingly pitting occurred after hydrogen charging, as shown in Fig. 2.

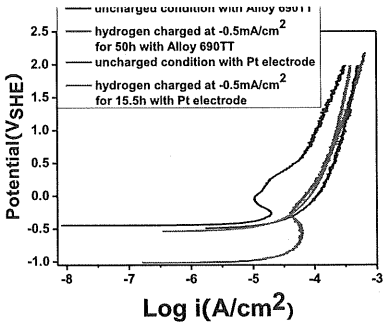


Fig. 1 Anodic polarization curves of uncharged and hydrogen charged at -0.5mA/cm$^2$ for 50h specimens in a simulated PWR water with 30cc/kg DH and containing 1200 ppm B in $H_3BO_3$ and 2 ppm Li in LiOH at 290°C, 9 MPa. The scan rate is 50mV/min.

### 3.2 Effects of hydrogen on the growth of oxide film

At 0.277$V_{SHE}$ (0.3$V_{Ag/AgCl}$) constant potential, the time reaching steady current density was 2300s, almost the same both for uncharged and charged conditions, as shown in Fig. 3. The steady current density of the charged sample was

16.670μA/cm$^2$ and that of uncharged samples was 13.03μA/cm$^2$. The results agreed with that displayed by anodic polarization, which implied that hydrogen charging increased anodic steady current density.

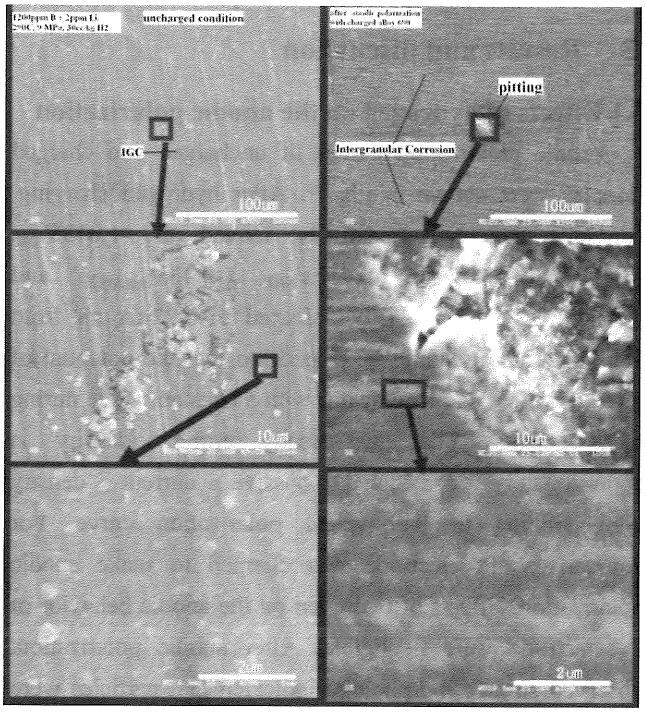


(a) (b)

Fig. 2 Surface morphologies after anodic polarization in the simulated water with 2.6ppm DH, containing 1200 ppm B in $H_3BO_3$ and 2 ppm Li in LiOH at 290°C, 9 MPa:(a) uncharged condition, (b) charged at -0.5mA/cm$^2$ for 50h

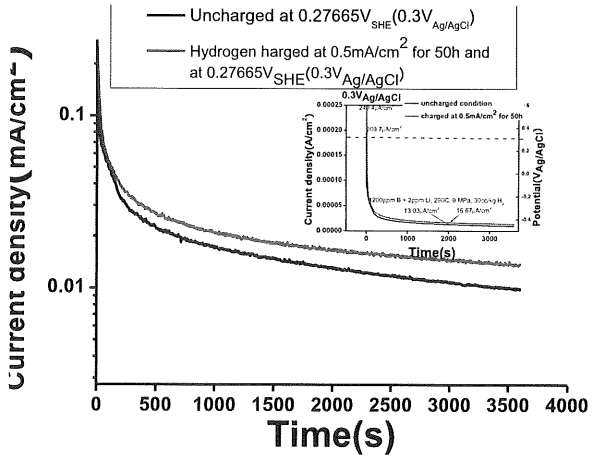


Fig. 3 Current density variations at 0.3 $V_{Ag/AgCl}$ with time for charged Alloy 690TT in the simulated PWR primary water with 2.6ppm DH, containing 1200 ppm B in $H_3BO_3$ and 2 ppm Li in LiOH at 290°C, 9 MPa.

### 3.3 Effects of hydrogen on the impedance response of oxide film

Fig.4 displayed the EIS data of Alloy 690TT, in the form of Nyquist diagram, of uncharged and charged samples in the testing solutions at open circuit potential. Only two semicircles were present and capacitance semicircle decreased especially in the range of medium and low frequencies. Different abscissa was mainly caused by the different solution between work electrode and reference electrode. The measured impedance spectra were analyzed by fitting method on the basis of the equivalent circuit, which was given in Fig. 5. The equivalent circuit consists of the series of the resistance of the outer oxide layer Rf1 in parallel to the capacitance of outer oxide layer C1 and the resistance of the inner oxide layer Rf2 in parallel to the constant phase element (CPE) of the inner oxide layer. CPE means a non-intuitive circuit element that was discovered (or invented) while looking at the response of present testing systems. Good agreement was obtained between the measured and fitted spectra at high and low frequencies, as shown in Figs. 4, 6. The calculated results of Rs, C, CPE, Rf were shown in Table I. At open circuit potential, charged hydrogen decreased capacitance both of outer oxide layer and inner oxide layer, increased resistance of outer oxide layer and decreased inner oxide layer. At 0.277V$_{SHE}$ (0.3V$_{Ag/AgCl}$) constant potential, charged hydrogen decreased both resistance and capacitance of outer oxide layer.

Table I values of Rs, C, CPE, Rf for oxide film on charged and uncharged Alloy 690TT in the simulated PWR primary water with 2.6ppm DH and containing 1200ppm B in $H_3BO_3$ and 2ppm Li in LiOH at 290°C, 9 MPa.

| E ($V_{Ag/AgCl}$) | | Rs (Ω.cm$^2$) | C1 (μF/cm$^2$) | Rf1 (Ω.cm$^2$) | CPE1-T (μF/cm$^2$) | CPE1 -P | Rf2 (Ω.cm$^2$) |
|---|---|---|---|---|---|---|---|
| 0 | ① | 608.4 | 0.01917 | 128.9 | 1864.4 | 0.57 | 877.3 |
| | ② | 616.4 | 0.01069 | 183.2 | 7457 | 0.56 | 292.5 |
| 0.3 | ① | 703.1 | 0.0083 | 207.2 | 1243.1 | 0.89 | 5261 |
| | ② | 608.8 | 0.01843 | 139.0 | 1288.4 | 0.81 | 7874 |

①—uncharged, ②—charged at -0.5mA/cm$^2$ for 50h

However, charged hydrogen had little effect on the resistance and capacitance of the inner oxide layer. It was implied that trapped hydrogen changed the electrochemical process during the growth of oxide film. It was generally

accepted that hydrogen could accelerate the dissolution and oxidation of iron [11, 12]. Especially, at OCP, the effects of hydrogen were complex since the electrochemical processes were the combination of anodic and cathodic reactions.

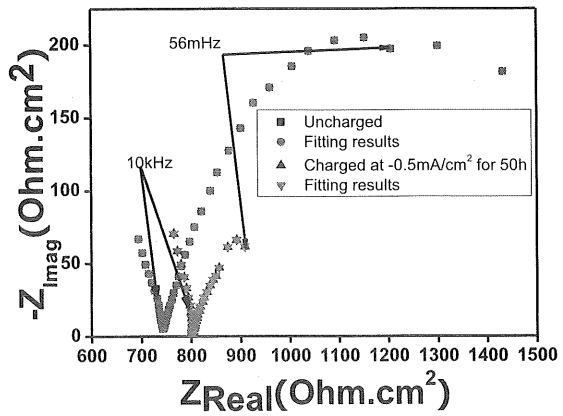


Fig 4 Impedance spectra behavior at open circuit potential on uncharged and hydrogen charged Alloy 690 TT preformed in simulated PWR primary water with 2.6ppm DH, containing 1200 ppm B in $H_3BO_3$ and 2 ppm Li in LiOH at 290°C, 9 MPa.

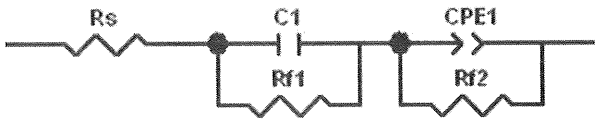


Fig. 5 The equivalent circuit for the oxide film on Alloy 690TT in the simulated PWR primary water with 2.6ppm DH, containing 1200 ppm B in $H_3BO_3$ and 2 ppm Li in LiOH at 290°C, 9 MPa.

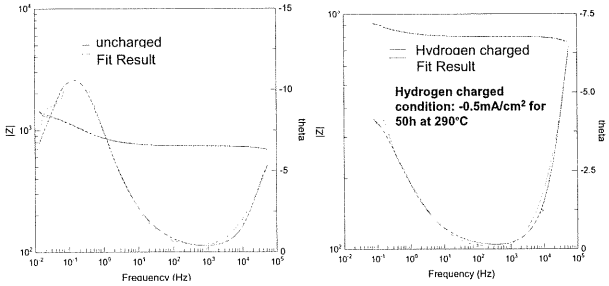


(a) (b)

Fig. 6 Comparison of experimental data for Alloy 690TT in the simulated PWR primary water with 2.6ppm DH, containing 1200ppm B in $H_3BO_3$ and 2ppm Li in LiOH at 290°C, 9 MPa. With the fitted data obtained by the equivalent circuit in Fig. 5.

### 3.4 Effects of hydrogen on electronic properties of oxide film

Fig. 7 showed the Mott-Schottky plots of the passive films on the uncharged and charged specimens at $0.277V_{SHE}$ ($0.3V_{Ag/AgCl}$). The slope of a Mott-Schottky plot was an indication of the conductivity type of the semiconductor. For uncharged condition, it can be concluded that the oxide film formed on Alloy 690TT were only n-type semiconductors due to the positive slope and donor density $N_D$ was $3.08\times10^{21}cm^{-3}$. After hydrogen charging, the donor density increased to $8.45\times10^{21}cm^{-3}$ and p-type semiconductor was present, which acceptor density $N_A$ was $5.31\times10^{21}cm^{-3}$. Therefore, the changing semiconductor of oxide film at $0.277V_{SHE}$ ($0.3V_{Ag/AgCl}$) seemingly was related to charged hydrogen.

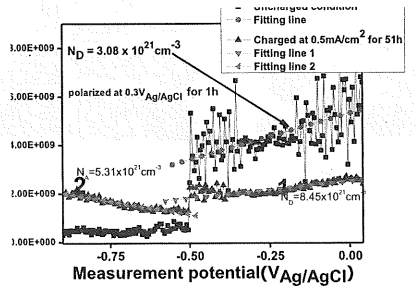


Fig. 7 Mott-Schottky plots of the passive films on uncharged and hydrogen charged Alloy 690TT at $-0.5mA/cm^2$ for 50h in the simulatd PWR primary water with 2.6ppm DH, containing 1200 ppm B in $H_3BO_3$ and 2 ppm Li in LiOH at 290°C, 9 MPa. The passive films were formed at $0.277V_{SHE}$ ($0.3V_{Ag/AgCl}$) for 2h before the Mott-Schottky plot measurements.

### 3.5 Depth profile of oxide film formed at $0.277V_{SHE}$ ($0.3V_{Ag/AgCl}$) by means of XPS analysis

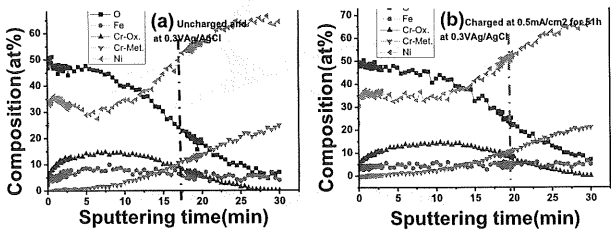


Fig. 8 Composition profiles in the depth of oxide film formed at $0.277V_{SHE}$ ($0.3V_{Ag/AgCl}$): (a) uncharged and (b) hydrogen charged at $-0.5mA/cm^2$ for 50h after exposure to the simulated PWR primary water with 2.6ppm DH,

containing 1200 ppm B in $H_3BO_3$ and 2 ppm Li in LiOH at 290°C, 9 MPa. Broken lines indicate film thickness, which was determined by the point which indicated the half oxygen content of the surface.

To confirm the effects of hydrogen on the properties of oxide film further, XPS analysis with depth profile sputtering was made. The results were shown in Figs. 8 to 10. The oxide film was composed of two layers, which Ni, Fe-enriched outer layer and Cr-enriched inner layer for both hydrogen charged and uncharged conditions. $SiO_2$ was used for calibration and the sputtering rate was about 6.06nm/min. Thickness of oxide films were equivalent to 17.4min and 19.6min sputtering time for uncharged and hydrogen charged samples, respectively. It is clear that the thicker film was formed after hydrogen charging.

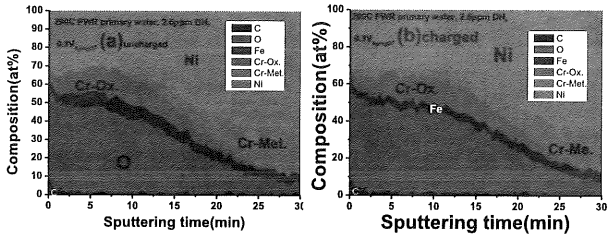


Fig. 9 Composition profiles in the depth of oxide film formed at $0.277V_{SHE}$ ($0.3V_{Ag/AgCl}$): (a) uncharged and (b) hydrogen charged at -0.5mA/cm$^2$ for 50h after exposure to the simulated PWR primary water with 2.6ppm DH, containing 1200 ppm B in $H_3BO_3$ and 2 ppm Li in LiOH at 290°C, 9 MPa.

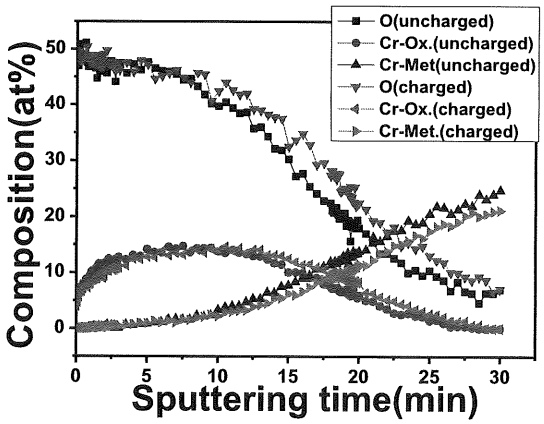


Fig. 10 O, $Cr_{Ox}$, $Cr_{Met}$ composition profiles in the depth of oxide film formed at $0.277V_{SHE}$ ($0.3V_{Ag/AgCl}$): (a) uncharged and (b) hydrogen charged after exposure to the simulated PWR primary water with 2.6ppm DH, containing 1200 ppm B in $H_3BO_3$ and 2 ppm Li in LiOH at 290°C, 9 MPa.

It was argued that the chemical states of nickel and iron would change during $Ar^+$ sputtering by S. Suzuki et al [13]. It was known that Cr played a key role during the growth of oxide film for its corrosion resistance. So, depth profile for two chemical states of Cr with sputtering time was especially displayed by Fig. 10. According to depth profile results, it was confirmed that hydrogen did not increase oxidation of chromium in the outer layer of oxide film, whereas, hydrogen maybe increased oxidation of chromium in the inner layer of oxide film.

## 4. Conclusion

The following were revealed from this study about the influence of hydrogen charging in the PWRs primary water at 290°C, using electrochemical measurements, and surface analysis:

1) Open circuit potential of Alloy 690TT decreased significantly after hydrogen charging at 290°C, 9 MPa, in hydrogenated PWRs primary water.

2) Hydrogen increased steady anodic current density of Alloy 690TT in hydrogenated PWRs primary water at 290°C. Hydrogen charging probably was the cause of pitting and slight IGA.

3) Hydrogen charging decreased capacitance loop, changed the electrochemical process in the growth of oxide film and brought different values of electrochemical elements.

4) Oxide film on hydrogen charged Alloy 690TT specimen formed at $0.277V_{SHE}$ ($0.3V_{Ag/AgCl}$) was thicker than that of uncharged specimen in the simulated PWR primary water with 2.6ppm DH and at 290°C. Hydrogen charging did not have significant effect on the oxidation of chromium in the outer layer of oxide film, but probably increased the oxidation of chromium in the inner layer of oxide film.


### Ackonwledgements

This work has been performed as a part of the PEACE-E program jointly supported by EDF, EPRI, SKI, TEPCO, TohokuEPCO, Chubu-EPCO, JAPCO, HITACHI Ltd., MHI, TOSHIBA Co., and IHI. This work has been performed under the support of Grant-in-Aid for Scientific Research (S)

17106002 and (C) 20560063, Japan Society for the Promotion of Science and partly supported by The Special Funds For The Major State Basic Research Projects G2006CB605000 in China. Prof. T. Yonezawa, Prof. Q. J Peng and Prof. Y. B Qiu are also appreciated for helpful discussion.

**Reference:**

[1] G. Ecomomy, R. J. Jacko, and F. W. Pement. Corrosion, 1987, vol. 43, pp. 737-733.

[2] N. Totsuka and Z. Szklarska-Smialowska. Corrosion, 1987, vol. 43, pp. 734-738.

[3] C. H. Shen and P. G. Shewmon. Metallurgical Transactions A, 1990, vol. 21A, pp. 1261-1271.

[4] D.S. Morton, S.A. Attanasio, G.A. Young, P.L. Andresen and T.M. Angeliu. Corrosion 2001, Houston, TX, NACE, 2001, paper no. 01117.

[5] P. L Andresen, J. Hickling, A. Ahluwalia, and J. Wilson. Corrosion, 2008, vol. 64, no. 9, pp. 707-720.

[6] J.B. Ferguson, H. F. Lopez. Metallurgical and Materials Transactions A, 2006, vol. 37 A, p. 2471.

[7] R. B. Rebak, F. H. Hua. "The role of Hydrogen and creep in Intergranular Stress Corrosion Cracking of Alloy 600 and Alloy 690 in PWR Primary Water Environments-a review", Envrionment Induced Cracking of Metals-2, 2004, UCRL-PROC-205679.

[8] A. Machet, A. Galtayries, P. Marcus, P. Combrade, P. Jolivet and P. Scott. Surface and Interface Analysis. 2002, 34, p197–200.

[9] T. Terachi1, N. Totsuka, T. Yamada, T. Nakagawa, H. Deguchi, M. Horiuchi and M. Oshitani. Journal of Nuclear Science and Technology, vol. 40, No. 7, p. 509–516.

[10] D. D. Macdonald, A. C. Scott, and P. Wentrcek. Journal of The Electrochemical Society, 1979, vol. 126, p. 908-911.

[11] L.J. Qiao, J.L. Luo. Corrosion, 1998, vol. 54(4), p. 281-288.

[12] Z. M. Zeng, J. L. Luo, and P. R. Norton. Journal of The Electrochemical Society, 2004, 151(6), p. B291-B298.

[13] S. Suzuki, K. Sugiyama, Y. Waseda. Journal of Surface Analysis, 2002, vol. 9, p. 455-458.